Carbohydrate Polymers 92 (2013) 269–275

Contents lists available at SciVerse ScienceDirect

Carbohydrate Polymers

journal homepage: www.elsevier.com/locate/carbpol

Removal of fluoride from drinking water by cellulose@hydroxyapatite nanocomposites

Xiaolin Yu, Shengrui Tong**, Maofa Ge*, Junchao Zuo

Beijing National Laboratory for Molecular Sciences (BNLMS), State Key Laboratory for Structural Chemistry of Unstable and Stable Species, Institute of Chemistry, Chinese Academy of Sciences, Beijing 100190, PR China

ARTICLE INFO

Article history:
Received 13 July 2012
Received in revised form 22 August 2012
Accepted 24 September 2012
Available online 1 October 2012

Keywords:
Cellulose
Nanocomposites
Fluoride
Adsorption

ABSTRACT

Cellulose@hydroxyapatite (HA) nanocomposites were prepared in NaOH/thiourea/urea/H_2O solution via situ hybridization. The composite materials combine the advantage of cellulose and HA with the high specific surface area and the strong affinity toward fluoride. The composite materials were characterized by FTIR, SEM, XRD, TG and XPS, and the adsorption of fluoride was investigated. Adsorption kinetics indicated the adsorption equilibrium of fluoride was within 360 min and the adsorption process was well described by the pseudo-second-order kinetic model. The Langmuir and Freundlich isotherm models could fit the experimental data well. At the initial fluoride concentration of 10 mg/L, the residual concentration using above 3 g/L adsorbent dose could meet the drinking water standard of WHO norms. Furthermore, the coexisting anions had no significant effect on fluoride adsorption.

1. Introduction

Fluoride in drinking water due to the serious threat to human health is one of the serious worldwide problems (Bhatnagar, Kumar, & Sillanpaa, 2011). Hydroxyapatite ($Ca_{10}(PO_4)_6(OH)_2$, HA) is the main constituent of teeth and bones, and fluoride can substitute for hydroxide ion within the HA crystal structure to form the fluorapatite ($Ca_5(PO_4)_3F$), which makes teeth and bones denser, harder and more brittle (Mohapatra, Anand, Mishra, Giles, & Singh, 2009). The excessive ingestion of fluoride in drinking water can cause dental fluorosis, even skeletal fluorosis, which are chronic diseases manifested by mottling of teeth in mild cases, softening of bones and neurological damage in severe cases (Fan, Parker, & Smith, 2003). According to the World Health Organization (WHO) norms, the permissible limit range of fluoride in drinking water is 0.5–1.5 mg/L (Zhang, He, & Xu, 2012). However, in many parts all over the world, such as India, China, United States and Mexico, the fluoride concentration in ground water has far excessed the drinking water standard value (Miretzky & Cirelli, 2011). Therefore, it is essential to remove the excess fluoride from drinking water.

Various methods have been applied to remove the excess fluoride from water, such as precipitation (Reardon & Wang, 2000), ion exchange (Meenakshi & Viswanathan, 2007), reverse osmosis (Ndiayea, Moulin, Dominguez, Millet, & Charbit, 2005), electrodialysis (Lahnid et al., 2008) and adsorption (Ahmed, 2011; Islam & Patel, 2011; Mohan, Sharma, Singh, Steele, & Pittman, 2012; Zhao et al., 2010). Amongst all the methods mentioned above, adsorption is recognized as the most effective approach for the removal of fluoride due to the low cost, high efficiency and environmental friendly behavior (Gu, Fang, & Deng, 2005; O'Connell, Birkinshaw, & O'Dwyer, 2008). Many adsorbents have been used for defluoridation, including activated alumina, carbonaceous materials, activated clay, rare earth oxides, titanium rich bauxite, zeolites and modified natural polymers, etc. (Bhatnagar et al., 2011; Miretzky & Cirelli, 2011; Mohapatra et al., 2009). However, some adsorbents lose the fluoride removal capacity at low fluoride concentration, while some others are relative expensive (Fan et al., 2003; Tian, Wu, Liu, et al., 2011). In terms of an excellent adsorbent, the main requirement is a high benefit cost ratio.

The composite materials as the adsorbents containing natural polymers and inorganic origin have attracted great attention due to their combined advantages. Cellulose is the most abundant renewable biopolymer on earth, and is a very promising raw material available at low cost to synthesize an adsorbent for defluoridation. HA, an inorganic mineral, has been proved to be a good adsorbent because of the low cost, availability and high defluoridation capacity (Fan et al., 2003; Sundaram, Viswanathan, & Meenakshi, 2009). Sundaram et al. (Sundaram, Viswanathan, & Meenakshi, 2008) synthesized a nano-scale HA by precipitation and used it to remove the fluoride from aqueous solution, and found that the adsorption capacity was 1.457 mg/L; Gao et al. (Gao et al., 2009) prepared a nano-size HA by decomposition of precursor, and then investigated the defluoridation ability of nano-size HA. It is found that the

* Corresponding author. Tel.: +86 10 62554518; fax: +86 10 62559373.
** Corresponding author. Tel.: +86 10 62558682; fax: +86 10 62559373.
E-mail addresses: tongsr@iccas.ac.cn (S. Tong), gemaofa@iccas.ac.cn (M. Ge).

0144-8617/$ – see front matter © 2012 Elsevier Ltd. All rights reserved.
http://dx.doi.org/10.1016/j.carbpol.2012.09.045

adsorption capacity of fluoride could reach 0.489 mg/g. However, due to the high specific surface area and nano scale, the agglomeration of nano-size HA is very serious, leading to the low adsorption capacity of fluoride. In order to overcome the agglomeration of nano-size HA, cellulose was used as the template to disperse the nano-size HA in the cellulose matrix for the preparation of the composite materials, which can combine the advantages of cellulose and HA.

In the present work, we synthesized cellulose@HA nanocomposites in NaOH/thiourea/urea/H_2O solution and then characterized them by FTIR, SEM, XRD, TG and XPS. The effects of contact time, pH, initial adsorption concentration and coexisting ions were investigated for the removal of fluoride from drinking water.

2. Materials and methods

2.1. Materials

Medical absorbent cotton cellulose was obtained from Jiaozuo league Hygiene group (China). Alkali cellulose is prepared by treating cotton cellulose with 20% (w/v) aqueous NaOH solution. Calcium chloride ($CaCl_2$), sodium dihydrogen phosphate (NaH_2PO_4), sodium hydrate (NaOH), urea, thiourea, sodium sulfate (Na_2SO_4), sodium nitrate ($NaNO_3$), sodium phosphate ($Na_3PO_4{\cdot}12H_2O$) and sodium fluoride (NaF) were all analytical grade supplied by local chemical agent suppliers. All the solvents and reagents were used without further purification.

2.2. Synthesis of cellulose@HA nanocomposites

A solution with NaOH/thiourea/urea/H_2O of 8:6.5:8:77.5 by weight was cooled to −12 °C. 3.3 g cotton cellulose was immediately added into the above solution under vigorous stirring for 5 min to obtain a cellulose solution. The obtained cellulose solution was used for the preparation of cellulose@HA nanocomposites.

The cellulose@HA nanocomposites were synthesized according to previous reported methods with major modification (Jia, Li, Ma, Sun, & Zhu, 2010). 4.4 g $CaCl_2$ and 3.76 g $NaH_2PO_4{\cdot}12H_2O$ were dissolved into 100 mL distilled water, and then the above solution was added into the obtained cellulose solution under vigorous stirring at 90 °C for 14 h. The obtained cellulose@HA was filtered, washed sequentially with distilled water, ethanol and acetone, and then dried in vacuum at 60 °C.

2.3. Characterization of cellulose@HA

A Tensor 27 Fourier transform infrared spectroscopy (FTIR) was used to verify the presence of functional groups in the adsorbent. The morphology of the samples was observed by Hitachi S-4300 scanning electron microscope (SEM) operating at 15 kV. X-ray photoelectron spectroscopy data (XPS) was obtained with an ESCALab220i-XL electron spectrometer from VG Scientific using 300 W AlKα radiation. The specific surface area was measured by nitrogen adsorption at 77 K (BET method) using an automated gas sorption analyzer (Quantachrome Instruments, autosorb-iQ). Thermogravimetric analysis (TGA) measurement was performed from room temperature to 650 °C in air at a 10 °C/min heating rate on a Q600 TA Instruments.

2.4. Adsorption experiments

The adsorption experiments were carried out in the shaking table at 200 rpm and 25 ± 1 °C using 150 mL shaking flasks containing fluoride solutions with different initial concentration. The effects of contact time, pH value, adsorption isotherms, adsorbent dose and coexisting ions on the equilibrium adsorption capacity were investigated. The adsorbent dose was kept as 1 g/L for all the experiments except for the adsorbent dose study. The pH values of the solution were adjusted by 0.1 mol/L HCl or NaOH. The fluoride concentration in the solution was analyzed using an ion chromatography (ICS-900, Dionex). The adsorption capacity q_e (mg/g) was calculated as described by the following equation

$$q_e = \frac{(C_0 - C_e)V}{m} \quad (1)$$

where C_0 (mg/L) is the initial fluoride concentration, C_e (mg/L) is the fluoride equilibrium concentration, V (L) is the volume of the fluoride solution and m (g) is the mass of adsorbent.

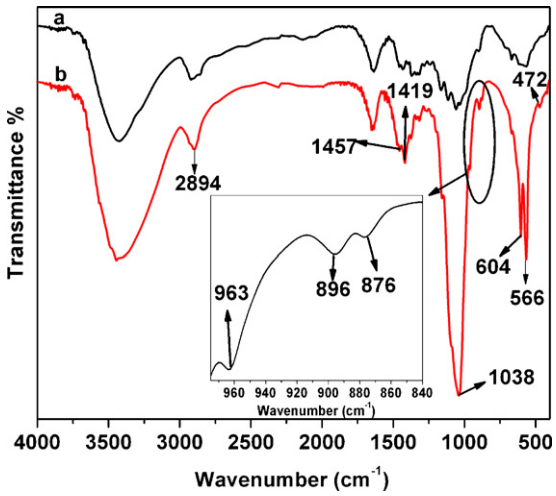

Fig. 1. FTIR spectra of native cellulose (a), and cellulose@HA (b).

3. Results and discussion

3.1. Characterization of cellulose@HA

The specific surface area of cotton cellulose and regenerated cellulose is 1.081 and 33.501 m^2/g. However, the specific surface area of cellulose@HA can reach 76.257 m^2/g, which is higher than that of cotton cellulose and regenerated cellulose. That is due to the formation of HA nanocomposites in the cellulose matrix.

The FTIR spectra of native cellulose and cellulose@HA are shown in Fig. 1. In the spectrum of native cellulose (Fig. 1a), typical peaks for many functional groups of cellulose can be observed. The adsorption band at 3424 cm^{-1} is attributed to the OH stretching vibration of cellulose and the other one at 2921 cm^{-1} corresponds to the C–H asymmetric and symmetric tensile vibration in pyranoid ring. The peak at 1636 cm^{-1} originates from the bending mode of the absorbed water. The band at 1372 cm^{-1} is due to the OH bending vibration. The adsorption peaks at 1433 cm^{-1}, 1164 cm^{-1}, 1114 cm^{-1}, 1058 cm^{-1} and 896 cm^{-1} relate to the CH_2 symmetric scissoring in pyranoid ring, C–O antisymmetric bridge stretching, the crystal absorption peak of cellulose I, C–O–C pyranoid ring skeletal vibration and the β-glycosidic linkages, respectively. These peaks are all the characteristic absorption bands of native cellulose (Liu, Zhang, Li, Yue, & Sun, 2010; Tian, Wu, Liu, et al., 2011). Compared with the spectrum of native cellulose (Fig. 1a), some typical characteristic peaks for HA in cellulose@HA (Fig. 1b) appear at 1038 cm^{-1}, 963 cm^{-1}, 604/566 cm^{-1} and 472 cm^{-1}, which are attributed to the ν_3 PO_4^{3-}, ν_1 PO_4^{3-}, ν_4 PO_4^{3-} and ν_2 PO_4^{3-}, respectively (Rehman & Bonfield, 1997). Furthermore, weak bands at 1457 cm^{-1}, 1419 cm^{-1} and 876 cm^{-1} correspond to ν_{3-3} CO_3^{2-}, ν_{3-4} CO_3^{2-} and ν_2 CO_3^{2-}, respectively, implying that the surface PO_4 sites of HA were partly replaced by carbonate ions (Hong et al.,

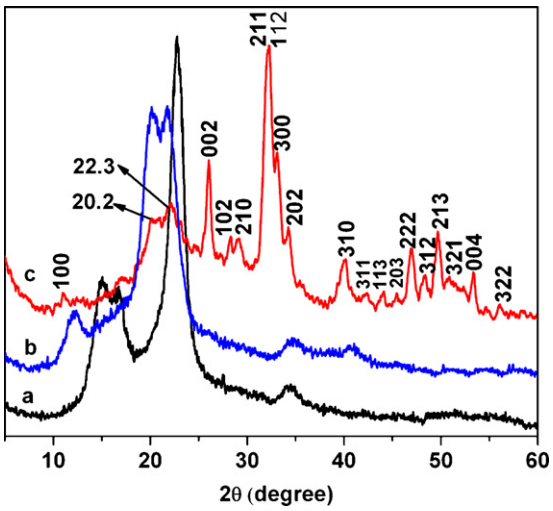

Fig. 2. XRD curves of cotton cellulose (a), alkali cellulose (b), and cellulose@HA (c).

2006; Islam, Mishra, & Patel, 2011; Rehman & Bonfield, 1997). Additionally, the bands of C–H asymmetric and symmetric tensile vibration in pyranoid ring at 2894 cm^{-1} and the β-glycosidic linkages at 896 cm^{-1} in cellulose@HA are still present, while other peaks of cellulose are hardly distinguishable, indicating the good extent and homogeneity of composite materials (Hong et al., 2006).

XRD curves of cotton cellulose, alkali cellulose and cellulose@HA are shown in Fig. 2. The diffraction curve of cotton cellulose presents four peaks at $2\theta = 14.8^\circ$ (1 0 1), 16.3° (1 0 $\bar{1}$), 22.7° (0 0 2), and 34.5° (0 4 0), which is a typical cellulose I (native cellulose) structure (Parikh, Thibodeaux, & Condon, 2007). After alkali treatment, the structure of native cellulose transforms from cellulose I to cellulose II, which can be proved by the appearance of characteristic peaks of cellulose II at $2\theta = 12^\circ$ (1 0 1), 19.8° (1 0 $\bar{1}$), and 21.7° (0 0 2) (Gurgel, de Freitas, & Gil, 2008). For cellulose@HA nanocomposites, the peaks at $2\theta = 20.2^\circ$ and 22.3° correspond to cellulose II and all the other peaks are assigned to the characteristic peaks of HA (JCPDS card no. 09-0432), indicating the formation of cellulose@HA nanocomposites. Moreover, the crystalline structure of HA is not affected by the presence of cellulose, implying that the interact binding between cellulose and HA exists in cellulose@HA nanocomposites (Nikpour, Rabiee, & Jahanshahi, 2012).

SEM images of cotton cellulose and cellulose@HA nanocomposites are shown in Fig. 3. Most of cotton cellulose fibers are 10–20 μm in diameter and the surface morphology of cotton cellulose looks smooth (Fig. 3a and c). However, the morphology of cellulose@HA has lost the fibrous structure and presents the irregular flakes (Fig. 3b and c). Furthermore, it is observed that the HA nanocrystallites is homogeneously dispersed in the cellulose matrix. As shown in the inset image in Fig. 3d, there are many small HA crystallites in the range of 20–50 nm. Due to enormous hydroxyl groups in cellulose and HA, hydrogen bonds can be formed between the cellulose and HA, which makes the combination of cellulose and HA perfect.

XPS analysis was used to analyze the surface composition of absorbent. As shown in Fig. 4, the photoelectron lines at a binding energy of about 285, 533, 349, 440, 134 and 190 eV attributed to C 1s, O 1s, Ca 2p, Ca 2s, P 2p and P 2s, respectively. The elemental ratio of Ca/P in cellulose@HA is 1.58, which is in reasonable agreement with the standard value of HA (1.67). This indicates that HA nanoparticles have dispersed successfully in the cellulose matrix. A new peak in fluoride-loaded cellulose@HA appears at 686.2 eV which is assigned to F 1S. Moreover, in fluoride-loaded cellulose@HA, the elemental ratio of Ca/P is 1.54 and the content of oxygen remarkably decreases from 38.19 atom % to 31.59 atom %. These reflect that the fluoride ion substitutes for hydroxide ion of HA to form the fluorapatite (Mohapatra et al., 2009).

The thermal stability of cotton cellulose and cellulose@HA nanocomposites was investigated using TGA. As shown in supplemental data Fig. S1, the first stage weight loss of cotton cellulose and cellulose@HA is observed below 200 °C, which is due to the evaporation of about 4% and 7% hydrated and coordinated water. The second stage from about 320 °C to 360 °C is attributed to the decomposition of cellulose. The third stage of cotton at around 510 °C is due to the oxidization of decomposition products (Liu, Fan, Dobashi, & Huang, 2002). For cellulose@HA, however, the loss of CO_3^{2-} also leads to the mass loss besides the oxidization of decomposition products (Jia et al., 2010). The residual weights of cotton and cellulose@HA are 0.4% and 51.5%, respectively. Thus, the excess amount of cellulose@HA suggests that the cellulose@HA nanocomposites are composed of at least 51.1% HA.

Supplementary material related to this article found, in the online version, at http://dx.doi.org/10.1016/j.carbpol.2012.09.045.

3.2. Adsorption properties

3.2.1. Adsorption kinetics

The effect of contact time for fluoride in aqueous solution is presented in supplemental data Fig. S2a. It is observed that the adsorption capacity of fluoride increases with the increasing contact time. Moreover, the initial adsorption rate is very fast and the adsorption equilibrium is established within 360 min for fluoride adsorption.

Supplementary material related to this article found, in the online version, at http://dx.doi.org/10.1016/j.carbpol.2012.09.045.

Adsorption kinetic model are usually used to explain the adsorption process and clear out the potential rate-limiting step. Thus, in this study, the pseudo-first-order kinetic model and the pseudo-second-order kinetic model are used to study the adsorption type and the mechanism.

The pseudo-first-order kinetic model is expressed as (Ho, Ng, & McKay, 2000):

$$q_t = q_e(1 - e^{-k_1 t}) \tag{2}$$

where q_t and q_e (mg/g) are the amount of solute at time t (min) and at equilibrium, respectively, and k_1 is the rate constant of the pseudo-first-order adsorption (min^{-1}).

The pseudo-second-order kinetic model (Chandra et al., 2010; Ho & McKay, 1999a) is described as:

$$q_t = \frac{k_2 q_e^2 t}{1 + k_2 q_e t} \tag{3}$$

The linearized form of the pseudo-second-order kinetic model can be expressed as:

$$\frac{t}{q_t} = \frac{1}{k_2 q_e^2} + \frac{1}{q_e} t \tag{4}$$

where q_t and q_e (mg/g) are the amount of solute at time t (min) and at equilibrium, respectively, and k_2 is the rate constant ($g\,mg^{-1}\,min^{-1}$).

When $t \to 0$, the initial adsorption rate h can be defined as follows:

$$h = k q_e^2 \tag{5}$$

where q_e (mg/g) is the amount of fluoride adsorbed at equilibrium, and k is the rate constant of the pseudo-second-order kinetic model ($g\,mg^{-1}\,min^{-1}$).

The curves of the pseudo-first-order kinetic model and the pseudo-second-order kinetic model are shown in supplemental data Fig. S2 and the kinetic parameters are calculated and

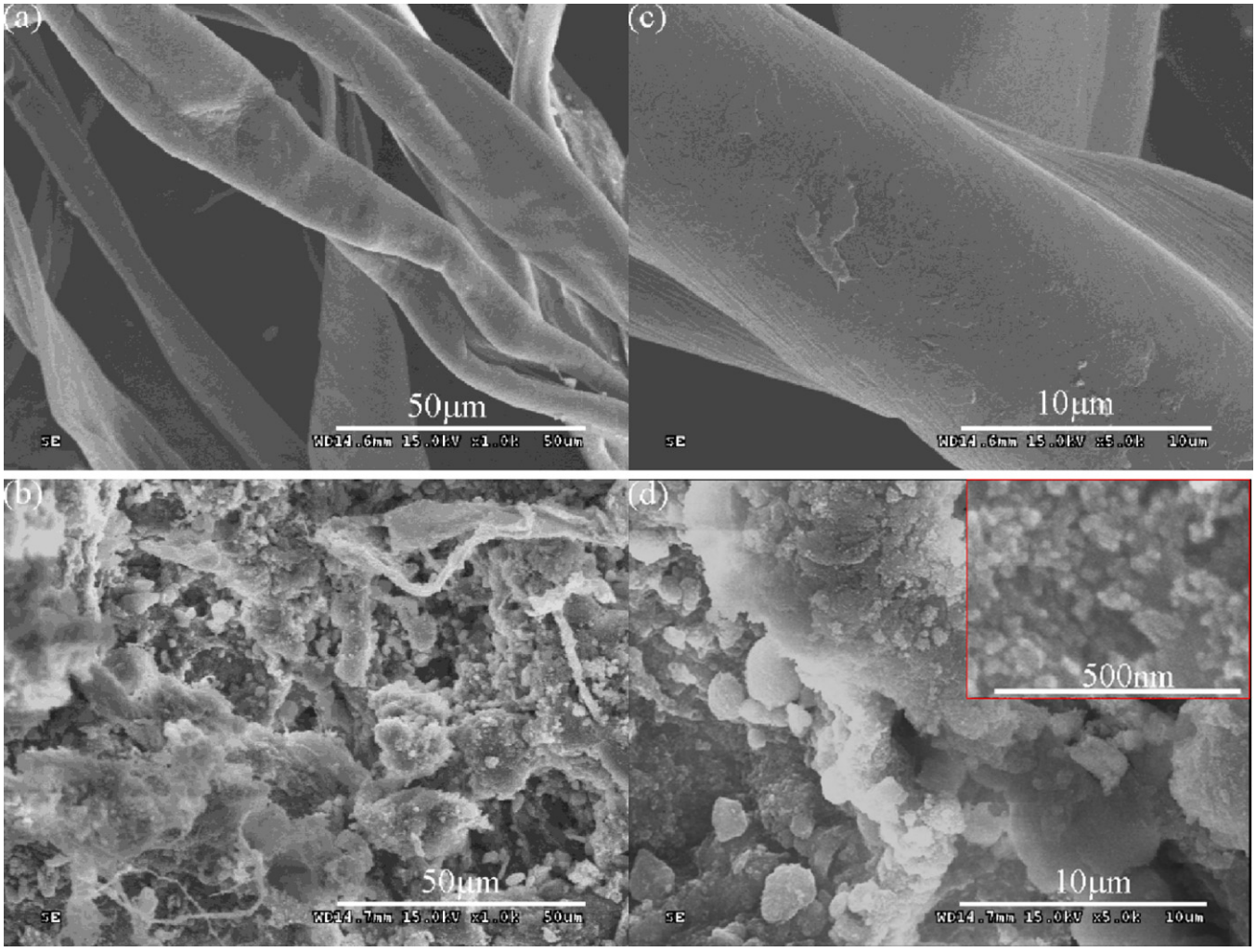

Fig. 3. SEM images of cotton cellulose (a, c) and cellulose@HA (b, d). Inset is enlarged image of cellulose@HA.

presented in supplemental data Table S1. The low correlation coefficient (R^2) of the pseudo-first-order kinetic model is obtained, indicating that the adsorption process cannot be explained by the pseudo-first-order kinetic model. This is owing to the fact that the pseudo-first-order kinetic model is only applicable at the initial stage (Ho & McKay, 1999b). Thus, it cannot fit well the whole adsorption process. However, the R^2 value of the pseudo-second-order kinetic model is very high and the theoretical value of $q_{e2(theo)}$ is in better agreement with the experimental $q_{e(exp)}$ values than $q_{e1(theo)}$. Thus, the adsorption process follows the pseudo-second-order kinetic model, which is more likely to predict the whole adsorption process. Moreover, the process may be a chemical adsorption process involving valence forces through sharing or exchange of electrons between adsorbent and adsorbate (Bulut & Tez, 2007) and the chemisorptions are the rate-limiting mechanism. Additionally, the initial adsorption rate h is 0.2883 mg g^{-1} min^{-1}.

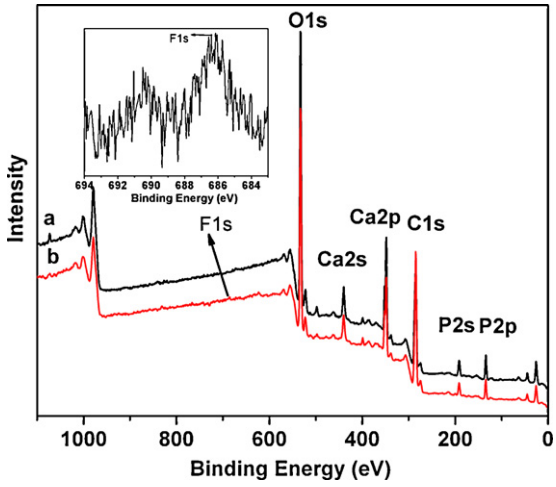

Fig. 4. The wide scan XPS spectra of cellulose@HA (a) and fluoride-loaded cellulose@HA (b). Inset is enlarged XPS spectrum of fluoride.

Supplementary material related to this article found, in the online version, at http://dx.doi.org/10.1016/j.carbpol.2012.09.045.

3.2.2. Effect of pH

One important factor in the fluoride removal is the aqueous solution pH, which can affect the adsorbent surface charge and the degree of ionization. As shown in Fig. 5, the concentration of PO_4^{3-} and the adsorption capacity of fluoride decrease with increasing pH. In terms of the PO_4^{3-} concentration, the HA nanocomposites may be partially dissolved at low pH, leading to the increase of PO_4^{3-} and Ca^{2+} concentration. Meanwhile, the adsorbent surface is positively charged due to the protonation and the dissolved Ca^{2+} concentration is high in the aqueous solution, which can react with F^- to form CaF_2 precipitate. Therefore, the adsorption capacity is

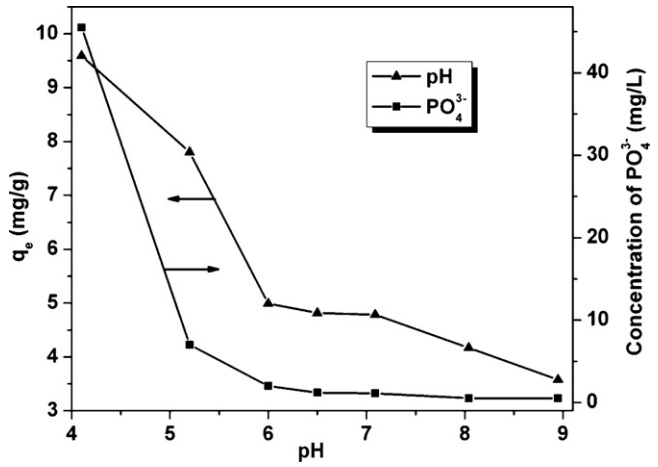

Fig. 5. Fluoride uptake and dissolved PO_4^{3-} concentration as a function of pH (initial concentration: 20 mg/L).

high at low pH value. With the increase of pH, the concentration of protons decreases and the adsorbent surface charge becomes negative. The electrostatic repulsion increases between fluoride and the adsorbent, which leads to the low adsorption capacity. Moreover, at pH >6.5, PO_4^{3-} can hardly be detected in the aqueous solution, indicating that the HA nanocomposites may not be dissolved. This suggests that there is no CaF_2 precipitate at this pH value in the aqueous solution. In order to avoid the HA dissolved, the optimum pH value is observed at 6.5.

3.2.3. Adsorption isotherms

The adsorption isotherm models of Langmuir and Freundlich are usually used to describe the relationship between the adsorbent and adsorbate. Langmuir isotherm model assumes a saturated molecular layer (monolayer) on the adsorbent surface, while Freundlich isotherms model assumes a heterogeneous surface and a multilayer adsorption with an energetic nonuniform distribution (Freundlich, 1906; Langmuir, 1918).

Langmuir isotherm model can be expressed as:

$$q_e = \frac{Q_{\max} b C_e}{1 + bC_e} \tag{6}$$

where C_e (mg/L) is the equilibrium concentration of fluoride in solution, q_e (mg/g) is the equilibrium adsorption capacity, Q_{max} (mg/g) is the maximum adsorption capacity per gram of sorbent, and b (L/mg) is the Langmuir constant related to the energy of adsorption. In this model, the dimensionless constant separation factor for equilibrium parameter (R_L) (Tian, Wu, Lin, Huang, & Huang, 2011) can be defined as:

$$R_L = \frac{1}{1 + bC_0} \tag{7}$$

where C_0 (mg/L) is the initial concentration of fluoride and b (L/mg) is the Langmuir constant. The value of R_L indicates the type of isotherm to be irreversible ($R_L = 0$), favorable ($0 < R_L < 1$), linear ($R_L = 1$) or unfavorable ($R_L > 1$).

Freundlich isotherm model can be expressed as:

$$q_e = K_f C_e^{1/n} \tag{8}$$

where C_e (mg/L) is the equilibrium concentration of fluoride in solution, q_e (mg/g) is the equilibrium adsorption capacity, K_f (mg/g) and n are Freundlich constants related to adsorption capacity and heterogeneity factor, respectively.

Supplemental data Fig. S3 shows the Langmuir and Freundlich isotherms for fluoride adsorption and the isotherm parameters are presented in Table 1. The correlation coefficients (R^2) of Langmuir and Freundlich isotherm models are larger than 0.98, indicating that both of the models can well explain the adsorption process of fluoride on cellulose@HA. The maximum adsorption capacity (Q_{max}) from Langmuir model is 4.2 mg/g, which is higher than that of nano-size HA (1.457 and 0.489 mg/g) reported by Sundaram et al. (Sundaram et al., 2008) and Gao et al. (Gao et al., 2009), respecitively. This result demonstrates that the cellulose template plays an important role in the fluoride adsorption. According to the Eq. (7), the values of R_L are in the range of 0.0177–0.1345, indicating that the adsorption process is favorable. Furthermore, the Freundlich constant n is greater than 1 which is a favorable condition for adsorption. This is consistent with the result of Langmuir model.

Table 1
Langmuir and Freundlich parameters for fluoride adsorption.

	Langmuir parameters		
	Q_{max} (mg/g)	b (L/mg)	R^2
F^-	4.20	3.08	0.98103
	Freundlich parameters		
	K_f (mg/g)	n	R^2
F^-	2.76	5.52	0.98705

Supplementary material related to this article found, in the online version, at http://dx.doi.org/10.1016/j.carbpol.2012.09.045.

3.2.4. Effect of adsorbent dose

The effect of adsorbent dose on the removal of fluoride is shown in Fig. 6. It is observed that the equilibrium concentration of fluoride decreases with increasing adsorbent dose. At lower adsorbent dose, the number of active adsorption site is less for the removal of fluoride. While due to the increase in the active sites with increasing the adsorption dose, the number of active site is sufficient for fluoride adsorption at high adsorbent dose. As shown in the inset figure, the fluoride equilibrium concentration can decrease below 1.5 mg/L at the initial concentration of 10 mg/L when adsorbent dose is above 3 g/L, which can fit the drinking water standard (below 1.5 mg/L) recommended by WHO norms. Moreover, when the adsorbent dose is above 4 g/L, the fluoride equilibrium concentration can reach around 0.8 mg/L, which is considered beneficial to human being in drinking water (Mohapatra et al., 2009). In order to clear out the property of the adsorbent surface, the distribution coefficient Kd is

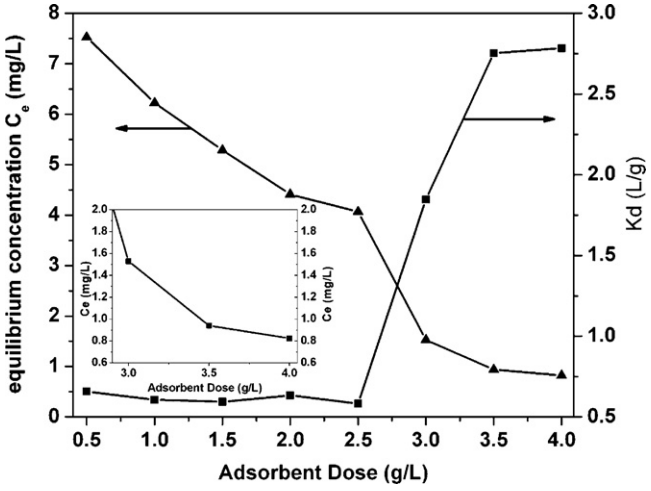

Fig. 6. Equilibrium concentration and Kd values of fluoride as a function of adsorbent dose (initial concentration: 10 mg/L, pH 6.5).

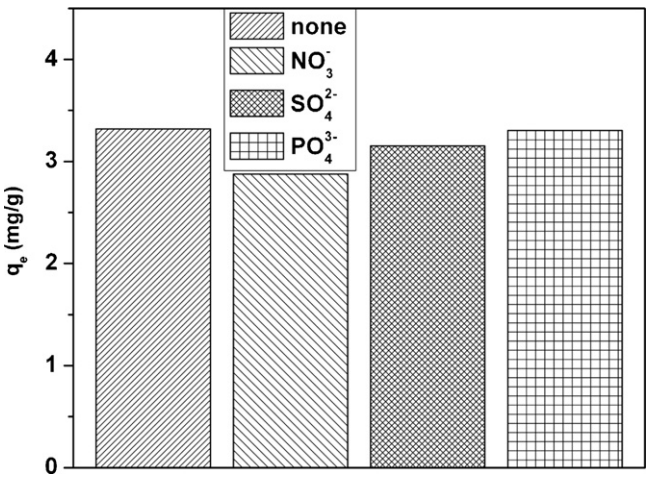

Fig. 7. Effect of coexisting ions for fluoride onto adsorbent (F^-: 5 mg/L, NO^{3-}, SO_4^{2-}, PO_4^{3-}: 10 mg/L; pH 6.5).

used, which describes the binding ability of adsorbent surface to an element. The *Kd* value can be expressed as:

$$Kd = \frac{(C_0 - C_e)V}{C_e m} \quad (9)$$

where C_0, C_e (mg/L) are the initial and equilibrium concentration of fluoride in solution, respectively, V (L) is the volume of the fluoride solution and m (g) is the mass of adsorbent. Tian et al. (Tian, Wu, Liu, et al., 2011) reported that *Kd* value for an element showed two different situations at a given pH value: if the surface was homogeneous, the *Kd* value stayed the same with adsorbent dose, whereas if the surface was heterogeneous, the *Kd* value would increase with increasing the adsorbent dose. As shown in Fig. 6, the *Kd* value stayed around 0.6 L/g when the adsorbent dose was below 2.5 g/L, implying that the surface of cellulose@HA is homogeneous; the *Kd* value increased with increasing the adsorbent dose when the adsorbent dose was above 2.5 g/L, indicating that the surface of cellulose@HA is heterogeneous.

3.2.5. *Effect of coexisting anions on fluoride adsorption*

Drinking water may contain several coexisting anions which can compete with fluoride for the adsorption sites. The effect of coexisting anions on fluoride adsorption was carried out in the presence of nitrate, sulfate and phosphate (10 mg/L each anion) at 5 mg/L initial fluoride concentration. As shown in Fig. 7, compared with the adsorption without coexisting anions, the coexisting anions have no significant effect on fluoride adsorption, indicating that cellulose@HA nanocomposites show the strong affinity for fluoride. The adsorption capacities of fluoride in the presence of the coexisting anions increase in the order of nitrate < sulfate < phosphate. The relative affinity of adsorbent for fluoride compared to other anions is likely to be related to the ionic radii. The order of ionic radii is fluoride (0.133 nm) < hydroxyl ion (0.137 nm) < nitrate (0.179 nm) < sulfate (0.230 nm) < phosphate (0.238 nm) (Marcus, 1988; Sternitzke et al., 2012). Due to the smaller ionic radii, fluoride ion fits better into the crystal structure of apatite and can substitute for hydroxyl ion in HA, yielding the more thermodynamic stable fluorapatite ($Ca_{10}(PO_4)_6F_2$), while other anions are too large to be easily accommodated (Aoba, 1997). Thus, the adsorption capacity of fluoride in the presence of coexisting anions is in the order of nitrate < sulfate < phosphate.

4. Conclusion

A cellulosic composite material as absorbent has been successfully prepared for efficient removal of fluoride from drinking water. The presence of cellulose facilitates the formation of nano-size HA and the interact binding between cellulose and HA exists in cellulose@HA nanocomposites. Cellulose@HA nanocomposites can be used as an efficient adsorbent for the fluoride removal. Adsorption kinetics indicates that the adsorption rate is rapid. The composite materials show a high adsorption capacity of fluoride compared with the nano-size HA. The residual fluoride concentration in drinking water can meet the drinking water standard of WHO norm using above 3 g/L adsorbent dose at the initial fluoride concentration of 10 mg/L. The coexisting anions have no significant effect on fluoride adsorption. Thus, cellulose@HA nanocomposites have a great potential as a novel adsorbent for the fluoride removal from drinking water.

Acknowledgement

This work was supported by the National Basic Research Program of China (973 Program, No. 2011CB933700) of Ministry of Science and Technology of China.

References

Ahmed, S. A. (2011). Batch and fixed-bed column techniques for removal of Cu(II) and Fe(III) using carbohydrate natural polymer modified complexing agents. *Carbohydrate Polymers*, *83*(4), 1470–1478.
Aoba, T. (1997). The effect of fluoride on apatite structure and growth. *Critical Reviews in Oral Biology & Medicine*, *8*(2), 136–153.
Bhatnagar, A., Kumar, E., & Sillanpaa, M. (2011). Fluoride removal from water by adsorption—a review. *Chemical Engineering Journal*, *171*(3), 811–840.
Bulut, Y., & Tez, Z. (2007). Adsorption studies on ground shells of hazelnut and almond. *Journal of Hazardous Materials*, *149*(1), 35–41.
Chandra, V., Park, J., Chun, Y., Lee, J. W., Hwang, I. C., & Kim, K. S. (2010). Water-dispersible magnetite-reduced graphene oxide composites for arsenic removal. *ACS Nano*, *4*(7), 3979–3986.
Fan, X., Parker, D. J., & Smith, M. D. (2003). Adsorption kinetics of fluoride on low cost materials. *Water Research*, *37*(20), 4929–4937.
Freundlich, H. (1906). Concerning adsorption in solutions. *Zeitschrift Fur Physikalische Chemie—Stochiometrie Und Verwandtschaftslehre*, *57*(4), 385–470.
Gao, S., Sun, R., Wei, Z. G., Zhao, H. Y., Li, H. X., & Hu, F. (2009). Size-dependent defluoridation properties of synthetic hydroxyapatite. *Journal of Fluorine Chemistry*, *130*(6), 550–556.
Gu, Z. M., Fang, J., & Deng, B. L. (2005). Preparation and evaluation of GAC-based iron-containing adsorbents for arsenic removal. *Environmental Science & Technology*, *39*(10), 3833–3843.
Gurgel, L. V. A., de Freitas, R. P., & Gil, L. F. (2008). Adsorption of Cu(II), Cd(II), and Pb(II) from aqueous single metal solutions by sugarcane bagasse and mercerized sugarcane bagasse chemically modified with succinic anhydride. *Carbohydrate Polymers*, *74*(4), 922–929.
Ho, Y. S., & McKay, G. (1999a). Pseudo-second order model for sorption processes. *Process Biochemistry*, *34*(5), 451–465.
Ho, Y. S., & McKay, G. (1999b). The sorption of lead(II) ions on peat. *Water Research*, *33*(2), 578–584.
Ho, Y. S., Ng, J. C. Y., & McKay, G. (2000). Kinetics of pollutant sorption by biosorbents: review. *Separation and Purification Methods*, *29*(2), 189–232.
Hong, L., Wang, Y. L., Jia, S. R., Huang, Y., Gao, C., & Wan, Y. Z. (2006). Hydroxyapatite/bacterial cellulose composites synthesized via a biomimetic route. *Materials Letters*, *60*(13–14), 1710–1713.
Islam, M., Mishra, P. C., & Patel, R. (2011). Arsenate removal from aqueous solution by cellulose-carbonated hydroxyapatite nanocomposites. *Journal of Hazardous Materials*, *189*(3), 755–763.
Islam, M., & Patel, R. (2011). Thermal activation of basic oxygen furnace slag and evaluation of its fluoride removal efficiency. *Chemical Engineering Journal*, *169*(1–3), 68–77.
Jia, N., Li, S. M., Ma, M. G., Sun, R. C., & Zhu, J. F. (2010). Hydrothermal synthesis and characterization of cellulose-carbonated hydroxyapatite nanocomposites in NaOH–urea aqueous solution. *Science of Advanced Materials*, *2*(2), 210–214.
Lahnid, S., Tahaikt, M., Elaroui, K., Idrissi, I., Hafsi, M., Laaziz, I., et al. (2008). Economic evaluation of fluoride removal by electrodialysis. *Desalination*, *230*(1–3), 213–219.
Langmuir, I. (1918). Adsorption of gases on plain surfaces of glass, mica platinum. *Journal of the American Chemical Society*, *40*, 1361–1403.
Liu, C. F., Zhang, A. P., Li, W. Y., Yue, F. X., & Sun, R. C. (2010). Succinoylation of cellulose catalyzed with iodine in ionic liquid. *Industrial Crops and Products*, *31*(2), 363–369.

Liu, N. A., Fan, W. C., Dobashi, R., & Huang, L. S. (2002). Kinetic modeling of thermal decomposition of natural cellulosic materials in air atmosphere. *Journal of Analytical and Applied Pyrolysis*, *63*(2), 303–325.

Marcus, Y. (1988). Ionic radii in aqueous solutions. *Chemical Reviews*, *88*(8), 1475–1498.

Meenakshi, S., & Viswanathan, N. (2007). Identification of selective ion-exchange resin for fluoride sorption. *Journal of Colloid and Interface Science*, *308*(2), 438–450.

Miretzky, P., & Cirelli, A. F. (2011). Fluoride removal from water by chitosan derivatives and composites: a review. *Journal of Fluorine Chemistry*, *132*(4), 231–240.

Mohan, D., Sharma, R., Singh, V. K., Steele, P., & Pittman, C. U. (2012). Fluoride removal from water using bio-Char, a green waste, low-cost adsorbent: equilibrium uptake and sorptiondynamics modeling. *Industrial & Engineering Chemistry Research*, *51*(2), 905–919.

Mohapatra, M., Anand, S., Mishra, B. K., Giles, D. E., & Singh, P. (2009). Review of fluoride removal from drinking water. *Journal of Environmental Management*, *91*(1), 67–77.

Ndiayea, P. I., Moulin, P., Dominguez, L., Millet, J. C., & Charbit, F. (2005). Removal of fluoride from electronic industrial effluent by RO membrane separation. *Desalination*, *173*(1), 25–32.

Nikpour, M. R., Rabiee, S. M., & Jahanshahi, M. (2012). Synthesis and characterization of hydroxyapatite/chitosan nanocomposite materials for medical engineering applications. *Composites Part B-Engineering*, *43*(4), 1881–1886.

O'Connell, D. W., Birkinshaw, C., & O'Dwyer, T. F. (2008). Heavy metal adsorbents prepared from the modification of cellulose: a review. *Bioresource Technology*, *99*(15), 6709–6724.

Parikh, D. V., Thibodeaux, D. R., & Condon, B. (2007). X-ray crystallinity of bleached and crosslinked cottons. *Textile Research Journal*, *77*(8), 612–616.

Reardon, E. J., & Wang, Y. X. (2000). A limestone reactor for fluoride removal from wastewaters. *Environmental Science & Technology*, *34*(15), 3247–3253.

Rehman, I., & Bonfield, W. (1997). Characterization of hydroxyapatite and carbonated apatite by photo acoustic FTIR spectroscopy. *Journal of Materials Science-Materials in Medicine*, *8*(1), 1–4.

Sternitzke, V., Kaegi, R., Audinot, J. N., Lewin, E., Hering, J. G., & Johnson, C. A. (2012). Uptake of fluoride from aqueous solution on nano-sized hydroxyapatite: examination of a fluoridated surface layer. *Environmental Science & Technology*, *46*(2), 802–809.

Sundaram, C. S., Viswanathan, N., & Meenakshi, S. (2008). Defluoridation chemistry of synthetic hydroxyapatite at nano scale: equilibrium and kinetic studies. *Journal of Hazardous Materials*, *155*(1–2), 206–215.

Sundaram, C. S., Viswanathan, N., & Meenakshi, S. (2009). Defluoridation of water using magnesia/chitosan composite. *Journal of Hazardous Materials*, *163*(2–3), 618–624.

Tian, Y., Wu, M., Lin, X., Huang, P., & Huang, Y. (2011). Synthesis of magnetic wheat straw for arsenic adsorption. *Journal of Hazardous Materials*, *193*, 10–16.

Tian, Y., Wu, M., Liu, R. G., Wang, D. Q., Lin, X. B., Liu, W. L., et al. (2011). Modified native cellulose fibers—a novel efficient adsorbent for both fluoride and arsenic. *Journal of Hazardous Materials*, *185*(1), 93–100.

Zhang, G., He, Z. L., & Xu, W. (2012). A low-cost and high efficient zirconium-modified-Na-attapulgite adsorbent for fluoride removal from aqueous solutions. *Chemical Engineering Journal*, *183*, 315–324.

Zhao, X. L., Wang, J. M., Wu, F. C., Wang, T., Cai, Y. Q., Shi, Y. L., et al. (2010). Removal of fluoride from aqueous media by Fe_3O_4@Al$(OH)_3$ magnetic nanoparticles. *Journal of Hazardous Materials*, *173*(1–3), 102–109.